ADV MATH SCI JOURNAL
Advances in Mathematics: Scientific Journal **11** (2022), no.11, 991–1017
ISSN: 1857-8365 (printed); 1857-8438 (electronic)
https://doi.org/10.37418/amsj.11.11.2

PARAMETER IDENTIFICATION PROBLEM TO FIND THE CARDIAC POTENTIAL WAVE FORM IN IONIC MODELS

Diogène Vianney Pongui Ngoma[1], Vital Delmas Mabonzo, Landry Jean Pierre Gomat, Germain Nguimbi, and Bervi Bienaime Bamvi Madzou

ABSTRACT. In this paper, we have defined an optimization problem allowing to directly find the shape of the cardiac wave of some ionic models. This allowed us to compare some of these ionic models via a parameter identification problem instead of comparing them directly by plotting the graphs for given values of the parameters. Compared to the empirical methods used to adjust one or two parameters at a time encountered in electrophysiology, we believe that our parameter identification approach is reliable and able to simultaneously identify four to eleven parameters of an ionic model. Using this approach, we adjusted the parameters of the Mitchell-Schaeffer and Aliev-Panfilov models to recover the shape of the action potential obtained experimentally by fluorescence.

1. INTRODUCTION

Several ionic models are available to describe the evolution of the potential across the membranes of cardiac cells. These models are generally read as a system coupled to highly nonlinear differential equations with many adjustable parameters. Parameters setting becomes more and more important to be able to customize these models from medical data (see for example [7,8]), to compare these

[1]*corresponding author*
2020 *Mathematics Subject Classification.* 49Mxx, 65Lxx, 34A12, 92B05.
Key words and phrases. Ionic models, optimal control, Nelder-Mead algorithm, parameter identification.

models with each other in the best possible way or to represent the most complex dynamic behavior of heart cells such as restitution properties. It is not easy to study the combined effect of parameter variation and the literature is generally not too explicit about how parameters are adjusted in ionic models. Parameters setting is possible with simpler ionic models using the totic formula relating parameters to phase durations [7, 9, 13]. Few attempts have been made to approach the parameters adjustment of an ionic model. In this article, we have explored the possibility of varying the cost functions and the influence this has on the quality of the identified parameters. Instead of defining a cost function that depends on values derived from the model solution (phase durations and wave speed) [11], we have defined a new cost function that depends directly on the solution of the Mitchell-Schaeffer model. This new parameter identification problem allowed us to directly find the shape of the cardiac wave with the standard Mitchell-Schaeffer ionic model [9] using as a cost function the square of the difference of the numerical and experimental potentials of the cardiac wave. Then we used the trapezium method to approximate this identification problem and carried out validation tests of the proposed numerical method. One of the undeniable advantages of this new approach is the flexibility in the ionic model choice. To demonstrate the flexibility of the approach, we have identified in the literature several usual ionic models in increasing order of complexity, namely the Aliev-Panfilov model, the modified Mitchell-Schaeffer model and the Fenton-Karma model ([1,3,15,16]), in the purpose of producing the action potential of each of these ionic models. We now know how to numerically solve each of these ionic models to produce an action potential, in itself an important advance for our work because it is far from easy to produce significant numerical solutions with these models. The originality of our approach compared to all that is published in the scientific literature consists in comparing ionic models via parameters identification problem instead of only drawing graphs for given values of the parameters. We have shown that it is possible to adjust the parameters of the Aliev-Panfilov model to recover almost perfectly the shape of the wave predicted by the standard Mitchell-Schaeffer model, and this in three different regions of the heart, ventricles, Purkinje fibers and atriums. We believe, we are the first to make optimal use of the parameter space to show that different ionic

can produce the same type of action potential. Using this approach, we also compared the Fenton-Karma models to the standard Mitchell-Schaeffer model. These two models give trans-membrane potentials with a different shape when plotted against time, but we were able to adjust their overall shape and in particular the phase durations. Then, we compared the standard Mitchell-Schaefffer model to that of Beeler-Reuter [2]. The potential generated by Beeler-Reuter admits a significantly more complex shape than that of standard Mitchell-Schaefffer, but we were able to adjust their overall shape. We also compared the modified Mitchell-Schaeffer model to the Beeler-Reuter model, which proved to be better than the standard Mitchell-Schaeffer model in approaching the complex form of the potential obtained by the Beeler-Reuter model. All these comparisons were made by adjusting the parameters of each of these models. Finally, we performed numerical simulations to adjust the parameters of the standard Mitchell-Schaeffer and Aliev-Panfilov models to find the shape of the action potential obtained by fluorescence on pigs at the Medical Biophysics Laboratory of the University of Toronto, Canada [10]. Once again, the validity of this approach testifies that the potential generated by standard Mitchell-Schaefffer fits better the potential obtained by fluorescence than that of Aliev-Panfilov. All our test cases illustrate the effectiveness of our parameter identification methods, at least for the ionic models with two or three variables

2. Optimization problem to find the shape of the cardiac wave

We now present a parameter identification method which tries to adjust the transmembrane potential $u = u(t)$ predicted by an ionic model (such as the Micthell-Schaeffer model) to the potential $\tilde{u} = \tilde{u}(t)$ measured experimentally or calculated using another ionic model. We minimize the function

$$J(\tau) = \frac{1}{2}\int_0^T \mid u(s,\tau) - \tilde{u}(s) \mid^2 ds, \tag{2.1}$$

where (u, v) is solution of the standard Mitchell-Schaeffer model:

$$\begin{cases} \dfrac{du}{dt} = f(u,v,\tau), \quad \text{with} \quad u(0,\tau) = u_0, \\ \dfrac{dv}{dt} = g(u,v,\tau), \quad \text{with} \quad v(0,\tau) = v_0, \end{cases} \tag{2.2}$$

with

$$f(u,v,\tau) = \frac{1}{\tau_{in}} v u^2 (1-u) - \frac{1}{\tau_{out}} u, \tag{2.3}$$

$$g(u,v,\tau) = \begin{cases} \dfrac{1-v}{\tau_{open}}, & \text{if} \quad u < u_{gate}, \\ \dfrac{-v}{\tau_{close}}, & \text{if} \quad u \geq u_{gate}. \end{cases} \tag{2.4}$$

$$\tau_{in} = 0.3\text{ms}, \quad \tau_{out} = 6\text{ms}, \quad \tau_{open} = 130\text{ms}, \quad \tau_{close} = 150\text{ms}, \quad u_{gate} = 0.13.$$

The function J is none other than the square of the norm in $L^2(0,T)$, that is $\| u - \tilde{u} \|^2_{L^2(0,T)}$. Minimizing J therefore comes to looking for the solution of (2.2) closest to $\tilde{u}$ in the sense of the norm $L^2(0,T)$.

2.1. **Numerical method used to find the shape of the wave.** We have used the Nelder-Mead method (as in [11]) to minimize the function $J = J(\tau)$ of the problem (2.1)-(2.2), while using the trapezoidal method [6] to approximate the integral (2.1):

$$J(\tau) \simeq \frac{\Delta t}{2} \left[(u_0 - \tilde{u}_0)^2 + 2 \sum_{i=1}^{N-1} (u_i - \tilde{u}_i)^2 + (u_N - \tilde{u}_N)^2 \right], \tag{2.5}$$

with $t_i = i\Delta t, i = 0, \ldots, N$ and $\Delta t = \dfrac{T}{N}$. The potential $\tilde{u} = \tilde{u}(s)$ is in general known for discete values $\tilde{u}_i, i = 0, \ldots, N$. It is therefore natural to approximate (2.1) by a quadrature formula. The values $u_i, i = 0, \ldots, N$, are none other than the approximations of the potential $u(t_i)$ obtained by the method of solving the system of ordinary differential equations (2.2).

2.2. **Validation test of the optimization method.** We want to validate our numerical approach. To do this, we will generate a potential $\tilde{u}$ (called here the "experimental" potential) with the standard Mitchell-Schaeffer model for the parameters $\tau^* = [0.3, 6, 130, 150]$. Then we will try to check if the numerical potential u obtained by minimizing the function $J = J(\tau)$ of the problem (2.1)-(2.2) totally covers the shape of $\tilde{u}$, that is to say $u = \tilde{u}$. Starting from the parameters τ_0 close to the parameter τ^* as initial condition, the Nelder-Mead method must produce a τ_{final} equal to τ^* when it converges. We set the tolerance of the method to within

10^{-4}. A value of $J(\tau_{final})$ close to zero guarantees that the adjustment of u on $\tilde{u}$ is good in the sense of least squares. The Table 1 gives the results corresponding to the test cases of validation of the method.

TABLE 1. Validation test Results of the optimization method.

τ_0	τ_{final}	$J(\tau_{final})$
$[0.27, 5.8, 127, 140]$	$[0.2998765, 5.9979534, 118.43252, 149.9954]$	0.0000003
$[0.2, 5.5, 125, 140]$	$[0.3, 6, 129.98955, 150.00001]$	$4.180D-13$
$[0.39, 8, 140, 170]$	$[0.3000001, 6.0000023, 130.00916, 150.00001]$	$4.620D-13$
$[0.29, 7, 120, 140]$	$[0.3000103, 6.00017, 130.98011, 150.00037]$	$1.498D-09$

Each row of the table 1 reads as follows, for example for the first line: starting from $\tau_0 = [0.27, 5.8, 127, 140]$ as initial condition, after 261 evaluations of the function J and 136 iterations of the Nelder-Mead method until convergence $\| \tau_{k+1} - \tau_k \| < 10^{-4}$ or $k > k_{max}$, we got $\tau_{final} = [0.2998765, 5.9979534, 118.43252, 149.9954]$ for which $J(\tau_{final}) = 0.0000003$. We notice in the table 1 that for initial values τ_0 quite close to the values of the parameter $\tau^* = [0.3, 6, 130, 150]$, we manage to calculate τ_{final} with a relative error $\frac{\mid \tau_{final} - \tau^* \mid}{\mid \tau^* \mid}$ of the order of 10^{-5} to within 10^{-6}, except for the first test case where $\tau_{final} = [0.2998765, 5.9979534, 118.43252, 149.9954]$. The potentials u and $\tilde{u}$ coincide, that is to say, we manage to overlap the two graphs for these two variables, as can be seen in Figure 1 (left and right graphs). The gate variables v and $\tilde{v}$ numerical and experimental, respectively, do not seem to coincide for all τ_0. This is not surprising because the function J contains a least squares term on u and not on v. The fact that $J(\tau_{final}) = 0$ at most to within 10^{-6} allows us to verify that we have correctly identified the parameters since this corresponds to a difference of at most 10^{-3} between u and $\tilde{u}$ in $L^2(0, T)$ norm, however without control over the adjustment of v.

3. VARIANT OF THE WAVE FORM FITTING PROBLEM.

Due to the difficulty of controlling the gate variable v, we added to the minimization function $J(\tau)$ in (2.1) a term of the least squares type depending on the numeric and experimental gate variables of the cardiac wave. This addition of a term to adjust only makes sense by adjusting the standard Mitchell-Schaeffer

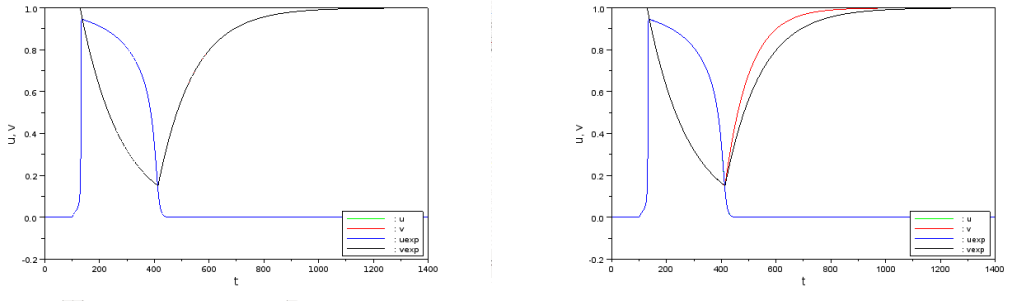

(A) $\tau_0 = [0.39, 8, 140, 170]$ (B) $\tau_0 = [0.25, 5.8, 128, 140]$

FIGURE 1. Graphs of (u, v) and $(\tilde{u}, \tilde{v})$ at convergence of the Nelder-Mead method

solution (u, v) to another solution of $(\tilde{u}, \tilde{v})$ standard Mitchell-Scheaffer. Otherwise, the gate variable $\tilde{v} = \tilde{v}(t)$ is a variable that represents the slow activity of a multitude ions and cannot be measured experimentally. Also, the gate variable $\tilde{v}$ of another two-variable model, such as the Aliev-Panfilov model (see below), will look completely different and cannot be adjusted with the v of the standard Mitchell-Schaeffer model. The minimization function becomes:

$$J(\tau) = \frac{1}{2}\int_0^T \mid u(s,\tau) - \tilde{u}(s) \mid^2 ds + \frac{1}{2}\int_0^T \mid v(s,\tau) - \tilde{v}(s) \mid^2 ds \tag{3.1}$$

where (u, v) is solution of the standard Mitchell-Schaeffer model:

$$\begin{cases} \dfrac{du}{dt} = f(u, v, \tau), \quad \text{with} \quad u(0, \tau) = u_0, \\ \dfrac{dv}{dt} = g(u, v, \tau), \quad \text{with} \quad v(0, \tau) = v_0. \end{cases} \tag{3.2}$$

Minimizing J means looking for the solution of (3.2) closest to $\tilde{u}$ and $\tilde{v}$ in the sense of the norm $L^2(0, T)$.

We discretize the function J by the trapezoidal method:

$$\begin{aligned} J(\tau) \simeq \frac{\Delta t}{2}\left[(u_0 - \tilde{u}_0)^2 + 2\sum_{i=1}^{N-1}(u_i - \tilde{u}_i)^2 + (u_N - \tilde{u}_N)^2\right] + \\ + \frac{\Delta t}{2}\left[(v_0 - \tilde{v}_0)^2 + 2\sum_{i=1}^{N-1}(v_i - \tilde{v}_i)^2 + (v_N - \tilde{v}_N)^2\right], \end{aligned} \tag{3.3}$$

with $t_i = i\Delta t, i = 0, \ldots, N$ and $\Delta t = \dfrac{T}{N}$. The potential $\tilde{u} = \tilde{u}(s)$ is generally known for discrete values $\tilde{u}_i, i = 0, \ldots, N$. It is therefore natural to approximate (3.1) by a quadrature formula. The values u_i and $v_i, i = 0, \ldots, N$, are none other than the approximations of the solution of $u(t_i)$ and $v(t_i)$ obtained by the ODE system resolution method (3.2).

By resuming the calculations of the table 1, with the new minimization function (3.1), we obtain the result of the table 2.

TABLE 2. Results of the Numerical method validation test.

τ_0	τ_{final}	$J(\tau_{final})$
$[0.27, 5.8, 127, 140]$	$[0.2999999, 5.9999981, 129.29997, 150]$	4.980D-12
$[0.2, 5.5, 125, 140]$	$[0.3000003, 6.0000051, 130.00001, 149.99997]$	4.774D-12
$[0.39, 8, 140, 170]$	$[0.3999990, 5.9999839, 130.00003, 149.99998]$	$8.093D-12$
$[0.29, 7, 120, 140]$	$[0.3000001, 6.0000016, 129.99995, 150]$	$6.853D-12$

By comparing table 1 and 2, we see that, for values of the parameter τ_0, sufficiently close to the values of the parameter $\tau^* = [0.3, 6, 130, 150]$, we manage to match u and $\tilde{u}$, v and $\tilde{v}$ two by two, and $\tau_{final} \approx \tau^*$ for all test cases in table 2. The graphs (left and right) in Figure 2 give the same results for different values of the parameter τ_0, with the graphs of the functions u and $\tilde{u}$ as well as v and $\tilde{v}$ which coincide perfectly.

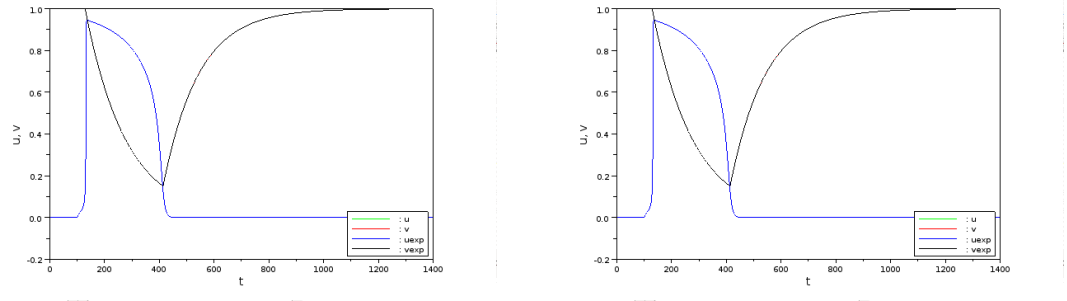

(A) $\tau_0 = [0.39, 8, 140, 170]$ (B) $\tau_0 = [0.25, 5.8, 128, 140]$

FIGURE 2. Graphs of solutions (u, v) and $(\tilde{u}, \tilde{v})$

4. VARIOUS IONIC MODELS

In this section we will present some ionic models and in the next section we will seek to compare these ionic models.

4.1. **Aliev-Panfilov model.**

The Aliev-Panfilov model [1] is an ionic model, composed of two ordinary differential equations which describe the dynamics of the trans-membrane potential u and a gate variable v,

$$\begin{cases} \dfrac{du}{dt} = ku(u-a)(1-u) - uv + I_{stim}, \\ \dfrac{dv}{dt} = -\varepsilon(u,v)(v + ku(u-a-1)) \end{cases} \tag{4.1}$$

where

$$\varepsilon(u,v) = \varepsilon_0 + \frac{\mu_1 v}{u+\mu_2}, \quad \tau_{AP} = [k, a, \varepsilon_0, \mu_1, \mu_2], I_{stim} = I_{stim}(t)$$

is an external stimulation current. The following values of parameters are given in [1]:

$$k = 8, a = 0.15, \varepsilon_0 = 0.002, \mu_1 = 0.2 \quad \text{and} \quad \mu_2 = 0.3.$$

The function $\varepsilon(u,v)$ is used to adjust the restitution curve of the Aliev-Panfilov model [**?**] to the experimental results, through the parameters μ_1 and μ_2. The Aliev-Panfilov model contains two time-dependent variables and five parameters like the standard Mitchell-Schaeffer model.

We used the $Scilab\ ode$ function to numerically calculate the solution of the Aliev-Panfilov model presented in Figure 3 with a stimulation current $I_{stim}(t) = 0.06$ for $t \in [100, 120]$, 0 everywhere else, and the initial condition $(u_0, v_0)^t \equiv (0,0)^t$. We set $T = 1200$ ms and computed the solution (u_i, v_i) for $i = 1, 2, \ldots, N$.

The potential u obtained for the Aliev-Panfilov model presents a slight peak followed by a short phase of repolarization at the beginning of the second phase (that is to say "the tray"). The standard Mitchell-Schaeffer model does not have this peak. Moreover, the representation of the gate variable v of the Aliev-Panfilov model admits a reversed form compared to that of standard Mitchell-Schaeffer, due to the fact that the state of equilibrium is $(u,v) = (0,0)$ for the Aliev-Panfilov model compared to $(u,v) = (0,1)$ for the standard Mitchell-Schaeffer. The variable v is not included between 0 and 1 for the Aliev-Panfilov model.

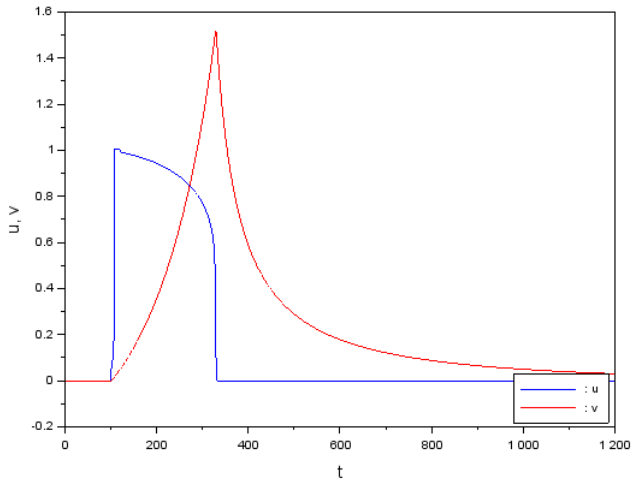

FIGURE 3. Representation of the trans-membrane potential u and the covering variable v as a function of time of the Aliev-Panfilov model, $\tau^{AP} = [8, 0.15, 0.002, 0.2, 0.3]$.

4.2. **Modified Mitchell-Schaeffer model.** The modified Mitchell-Schaeffer model [15,16] is an ionic model, composed of three ordinary differential equations which describe the dynamics of the trans-membrane potential $u(t)$, of the gate variable $v(t)$ and the concentration $c(t)$. This modified Mitchell-Schaeffer model is composed of ten parameters (see table 3):

- the equation for the trans-membrane potential u is the sum of three currents: the incoming current $I_{in} = I_{in}(u, v, c)$, the outgoing current $I_{out} = I_{out}(u)$ and the external stimulation current $I_{stim} = I_{stim}(t)$. This equation is written

$$\frac{du}{dt} = I_{in}(u, v, c) + I_{out}(u) + I_{stim}(t) \tag{4.2}$$

where the current I_{out} is a linear current and is defined by $I_{out}(u) = -\frac{u}{\tau_{out}}$, the current I_{in} is a nonlinear current which is the sum of two concentrations (independent and dependent)

$$I_{in}(u, v, c) = \frac{uv}{\tau_{in}}\{\phi_{ci}(u) + \beta e^{-c}\phi_{cd}(u)\} \quad \text{avec} \quad \beta > 0 \quad \text{constant.} \tag{4.3}$$

The equation (4.3) is justified by the fact that the accumulation of charges in the cell weakens the current towards the interior, thus reducing the variation of the action potential u. The behavior of the modified Mitchell-Schaeffer model is not sensitive to the form of the functions $\phi_{ci}(u)$ and $\phi_{cd}(u)$ which can be taken as linear in pieces, that to say:

$$\phi_{ci}(u) = \begin{cases} \dfrac{u}{u_{gate}} & \text{if} \quad u \leq u_{gate}, \\ 1 & \text{if} \quad u_{gate} < u \leq 1 - u_{gate}, \\ \dfrac{(1-u)}{u_{gate}} & \text{if} \quad 1 - u_{gate} < u, \end{cases}$$

and

$$\phi_{cd}(u) = \begin{cases} 0 & \text{if} \quad u \leq u_{gate}, \\ 1 - \dfrac{\mid 1 - 2u \mid}{1 - 2u_{gate}} & \text{if} \quad u_{gate} < u \leq 1 - u_{gate}, \\ 0 & \text{if} \quad 1 - u_{gate} < u. \end{cases}$$

- the equation for the gate variable v is defined as follows:

$$\frac{dv}{dt} = \begin{cases} \dfrac{(1-v)}{\tau_{open}} & \text{if} \quad u \leq u_{gate}, \\ \dfrac{-v}{\tau_{close}(u)} & \text{if} \quad u > u_{gate}, \end{cases} \tag{4.4}$$

with

$$\frac{1}{\tau_{close}(u)} = \begin{cases} \dfrac{1}{\tau_{fclose}} - \left(\dfrac{1}{\tau_{fclose}} - \dfrac{1}{\tau_{sclose}}\right)\left(\dfrac{1-u}{1-u_{sldn}}\right) & \text{if} \quad u > u_{sldn}, \\ \dfrac{1}{\tau_{sclose}} & \text{if} \quad u \leq u_{sldn}, \end{cases} \tag{4.5}$$

where $\tau_{fclose}, \tau_{sclose}$ and u_{sldn} are fast close, slow close and slow down potential, respectively.

- the concentration equation is characterized by a current, noted $I(t)$, which leads to the accumulation of charge in the cell and a linear current which attenuates the cell charge according to a time constant τ_{pump}. This equation is written:

$$\frac{dc}{dt} = -I(t) - \frac{c}{\tau_{pump}} \tag{4.6}$$

with

$$I(t) = \begin{cases} \dfrac{\varepsilon}{1-u_{gate}}\,(I_{in}+I_{out}) & \text{if} \quad u > u_{gate} \quad \text{and} \quad \dfrac{du}{dt} > 0, \\ 0 \qquad\qquad \text{else} \end{cases} \tag{4.7}$$

where currents I_{in} and I_{out} are defined in (4.2) and (4.3).

TABLE 3. Parameters of Modified Mitchell-Schaeffer Ionic Model.

Parameters	Values	Units
τ_{in}	0.28	ms
τ_{out}	3.2	ms
β	7.3	
u_{gate}	0.13	
u_{sldn}	0.89	
τ_{open}	500	ms
τ_{fclose}	22	ms
τ_{sclose}	320	ms
τ_{pump}	30000	ms
ε	0.033	

The solution (see Figure 4) of the modified Mitchell-Schaeffer model was obtained numerically using the $Scilab\ ode$ function with a stimulation current $I_{stim} = 0.004$ for $t \in [100, 150]$, and 0 everywhere else, starting from the initial condition $(u_0, v_0, c_0)^t \equiv (0, 0.99, 1.5)^t$. We set $T = 1400$ ms, and used the parameters defined in the Table 3.

Compared to the standard Mitchell-Schaeffer model, note the changes in the trans-membrane potential u, that to say a peak followed by early repolarization at the beginning of the tray period (observed for certain cardiac cells such as Purkinje fibers) as well as the much more abrupt return to equilibrium at the end of the treshold phasis. The gate variable v behaves quite differently with the modified Mitchell-Schaeffer model compared to the standard Mitchell-Schaeffer, although the equilibrium value for it is still 1.

4.3. **Fenton-Karma model.** The Fenton-Karma model [3, 17] is an ionic model, composed of eleven parameters (see table 4) and three ordinary differential equations that describe the dynamics of the trans-membrane potential u and two gate

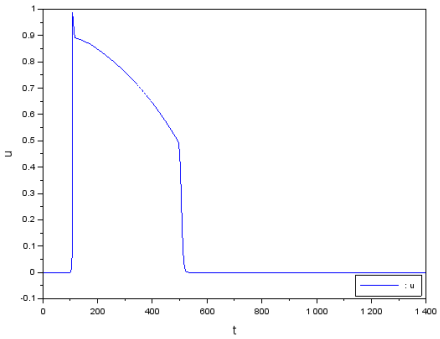

(A) Trans-membrane potential, u

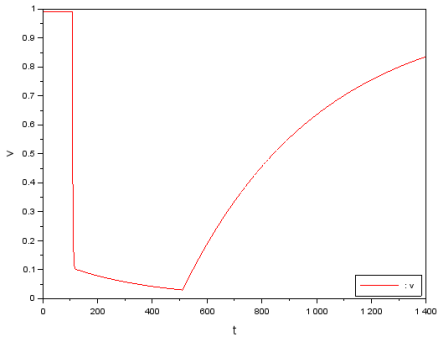

(B) gate variable v

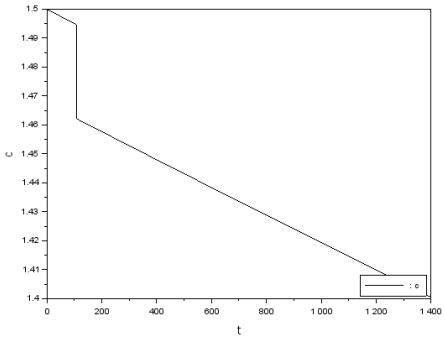

(C) Concentration c

FIGURE 4. Representation of trans-membrane potential (a), gate variable (b) and concentration (c) as a function of time of the modified Mitchell-Schaeffer model, with $\tau^{MSm} = [\tau_{in}, \tau_{out}, \beta, u_{gate}, u_{sldn}, \tau_{open}, \tau_{fclose}, \tau_{sclose}, \tau_{pump}, \varepsilon]$ given in table 3.

variables v and w for fast and slow ion channel closures, respectively. More precisely,

- the equation defining the trans-membrane potential u, is given by:

$$\frac{du}{dt} = -\left(I_{fast} + I_{slow} + I_{ung} + I_{stim}\right) \tag{4.8}$$

such that

1. I_{fast} is a fast in-cell current, defined by

$$I_{fast} = -v\frac{Q(u)}{\tau_{fast}}$$

where τ_{fast} is the fast depolarization time and $Q(u)$ is a piecewise linear function depending on the trans-membrane potential u,

$$Q(u) = \begin{cases} (1-u_{gate})(1-u) & \text{if} \quad u \geq u_{gate}, \\ 0 & \text{if} \quad u < u_{gate}. \end{cases} \tag{4.9}$$

2. I_{slow} is a slow current in the cell, defined by

$$I_{slow} = -w\frac{s(u)}{\tau_{slow}},$$

where τ_{slow} is the characteristic time related to the tray phase and $s(u)$ is a regular function

$$s(u) = \frac{1}{2}\left\{1 + \tanh(k(u-u_{sig}))\right\}. \tag{4.10}$$

3. I_{ung} is a ungated current favoring the passage of ions in the cell, given by

$$I_{ung} = \frac{P(u)}{\tau_{ung}},$$

where τ_{ung} is the passage time of ions in the cell and $P(u)$ is a piecewise linear function depending on the trans-membrane potential u and the critical exit potential u_{out}

$$P(u) = \begin{cases} 1 & \text{if} \quad u \geq u_{out}, \\ \dfrac{u}{u_{out}} & \text{if} \quad u < u_{out}. \end{cases} \tag{4.11}$$

- The equation defining the gate variable v for fast closing is given by

$$\frac{dv}{dt} = \frac{(v_\infty(u) - v)}{\tau_v(u)} \tag{4.12}$$

where

$$\begin{cases} v_\infty(u) = 0 \quad \text{and} \quad \tau_v(u) = \tau_{vclose} \quad \text{if} \quad u \geq u_{gate}, \\ v_\infty(u) = 1 \quad \text{and} \quad \tau_v(u) = \tau_{vopen} \quad \text{if} \quad u < u_{gate}. \end{cases} \tag{4.13}$$

- The equation defining the gate variable w for slow closing is defined by

$$\frac{dw}{dt} = \frac{(w_\infty(u) - w)}{\tau_w(u)} \tag{4.14}$$

where

$$\begin{cases} w_\infty(u) = 0 \quad \text{and} \quad \tau_w(u) = \tau_{wclose} \quad \text{if} \quad u \geq u_{gate}, \\ w_\infty(u) = 1 \quad \text{and} \quad \tau_w(u) = \tau_{wopen} \quad \text{if} \quad u < u_{gate}. \end{cases} \tag{4.15}$$

TABLE 4. Fenton-Karma Ionic Model Parameters [3, 17].

Parameters	Values	Units
τ_{fast}	0.25	ms
τ_{slow}	127	ms
τ_{ung}	130	ms
u_{out}	0.1	
τ_{vclose}	10	ms
τ_{vopen}	18	ms
τ_{wclose}	1000	ms
τ_{wopen}	80	
u_{gate}	0.13	
u_{sig}	0.85	
k	10	

The solution (see Figure 5) of the Fenton-Karma model was obtained numerically using the $Scilab\ ode$ function with a stimulation current $I_{stim}(t) = 0.08$ for $t \in [100, 102]$, and zero everywhere else, starting from the initial condition $(u_0, v_0, w_0)^t = (0.001, 0.99, 0.99)^t$. We set $T = 1200$ ms, and used the parameters defined in Table 4.

The trans-membrane potential u obtained with the Fenton-Karma model resembles that given by the Mitchell-Schaeffer model with the main difference being that u is closer to 1 at the beginning of the comparative tray to the Mitchell-Schaeffer u potential. The gate variable w behaves similarly to the gate variable v of the Mitchell-Schaeffer model, except that w decreases linearly while the Mitchell-Schaeffer v decreases exponentially. Note also that the amplitude of the variation of w is less than that of the Mitchell-Schaeffer gate variable v. The Fenton-Karma gate variable v has no equivalent in the Micthell-Schaeffer model. This variable represents a rapid dynamic of the ion channels, that to say a sudden exponential variation during the depolarization and repolarization phases, then a constant value throughout phase 2 of the potential action.

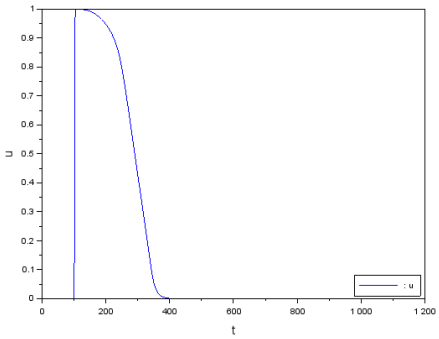

(A) Trans-membrane potential, u

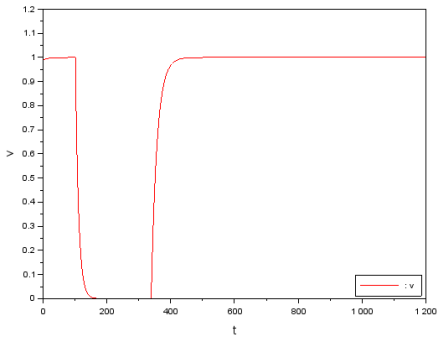

(B) gate variable v

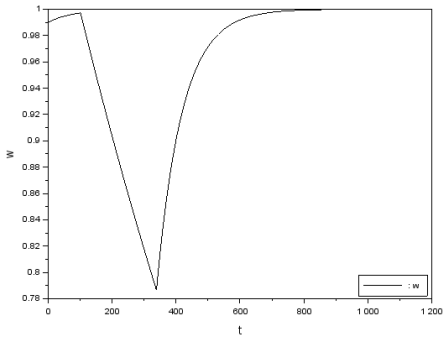

(C) slow gate variable w

FIGURE 5. Representation of trans-membrane potential (a), fast gate variable (b) and slow gate variable (c) as a function of time for the Fenton-Karma model, $\tau^{FK} = [\tau_{fast}, \tau_{slow}, \tau_{ung}, u_{out}, \tau_{vclose}, \tau_{vopen}, \tau_{wclose}, \tau_{wopen}, u_{sig}, k]$ according to Table 4.

5. COMPARISON OF IONIC MODELS

In this section we will seek to develop a technique for adjusting the parameters in order to compare the different ionic models presented in the section 4. To do this we will consider the optimization problem defined in the section 2, that to say the function of least squares type on the potential only:

$$J(\tau) = \frac{1}{2}\int_0^T \mid u(s,\tau) - \tilde{u}(s) \mid^2 ds. \tag{5.1}$$

The function J is approximated numerically by the trapezium method

$$J(\tau) \simeq \frac{\Delta t}{2}\left[(u_0-\tilde{u}_0)^2+2\sum_{i=1}^{N-1}(u_i-\tilde{u}_i)^2+(u_N-\tilde{u}_N)^2\right], \tag{5.2}$$

where u and $\tilde{u}$ are the trans-membrane potentials obtained by two different ionic models of section 4. For example, if we want to fit the Mitchell-Schaeffer model to the Aliev-Panfilov model, we will take $\tilde{u}$ as the trans-membrane potential predicted by Aliev-Panfilov (for given values of the parameters τ^{AP} of this model) then u as predicted by Mitchell-Schaeffer. The parameter to be identified will then be the $\tau = \tau^{MS}$ of the Mitchell-Schaeffer model. The J function only takes into account the potential u because there is no reason to be able to adjust the gate variables, these not being defined in the same way from one model to another. We will still discuss the behavior of the gate variables because it will be interesting to understand how the cell returns to equilibrium. Indeed, the gate variables influence the duration of the recovery period at the end of the potential action.

5.1. **Comparison of standard Mitchell-Schaeffer and Aliev-Panfilov ionic models.** The idea here is to start with the solution obtained (see figure 6) by the standard Mitchell-Schaeffer model, then try to identify the parameters of the Aliev-Panfilov model by minimizing the function (5.2) in order to adjust the potential predicted by Aliev-Panfilov to that predicted by the standard Mitchell-Schaeffer model for the values of $\tau^{MS} = [0.3, 6, 130, 150]$. Starting from $\tau_0^{AP} = [9, 0.11, 0.002, 0.02, 0.4]$ as the initial condition of the Nelder-Mead algorithm, we obtained

$$\tau_{final}^{AP} = [0.82578226, 0.0508103, 0.0102062, 0.1319747, 0.9004079],$$

for which

$$J(\tau_{final}^{AP}) = 0.1298053.$$

We notice that since the value of the least-squares function $J(\tau_{final}^{AP})$ is relatively small, fitting the Aliev-Panfilov potential u to the potential $\tilde{u}$ of Mitchell-Schaeffer standard is good. This is confirmed by the quasi-superposition of the graphs of potentials u for the two models, as illustrated in figure 6. Of course, the fit cannot be as good as for the validation test where the standard Mitchell-Schaeffer

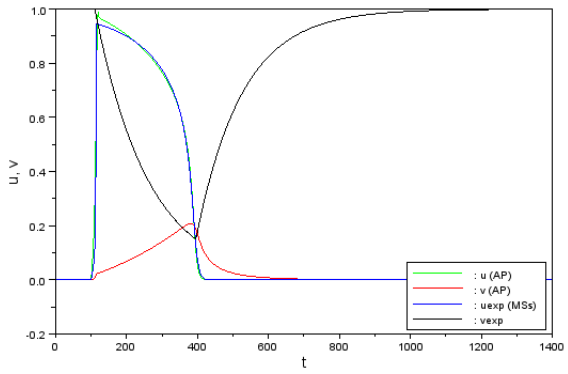

FIGURE 6. Graph illustrating the fitting of the Aliev-Panfilov model to the standard Mitchell-Schaeffer model.

model was fitted to a solution $\tilde{u}$ of the standard Mitchell-Schaeffer model, and for which $J < 10^{-5}$. The fact that the solutions u and $\tilde{u}$ of Aliev-Panfilov and Micthell-Schaeffer, respectively, fit well on each other, allows us to affirm that we have correctly identified parameters. It therefore seems that the dynamics of the trans-membrane potential described by the standard Mitchell-Schaeffer model can be reproduced with the Aliev-Panfilov model. Note however that the return to equilibrium of the recovery variables v predicted by the Mitchell-Schaeffer and Aliev-Panfilov models does not occur at the same speed. Indeed, the Aliev-Panfilov model predicts a phase 4 (from the end of repolarization to the return of v to equilibrium) between $T_4 = 400\ ms$ and $T_5 = 700\ ms$ (a duration $\Delta T_4 = 300\ ms$) while Mitchell-Schaeffer predicts such a phase between T_4 =400 ms and T_5 =1200 ms (a duration $\Delta T_4 = 800\ ms$)(in [11]).

5.2. **Adjustment of the Aliev-Panfilov model in three cardiac tissues.** We want to see if it is possible to adjust the Aliev-Panfilov model to recover the shape of the action potential in three cardiac tissues, namely the ventricle, the atrium and the Purkinje fibers. The idea here is to start with the solutions obtained in these three different cardiac regions (in [11]) using the standard Mitchell-Schaeffer model and then to adjust the trans-membrane potential predicted by the Aliev-Panfilov model to that of Mitchell-Schaeffer (see figure 7). For this, we identify the parameters of the Aliev-Panfilov model by minimizing the function $J = J(\tau)$ given in

(5.2). Starting from the initial conditions τ_0^{AP}, we obtained the results of the table 5 for the three cardiac tissues.

TABLE 5. Results of the identification problem for the three cardiac tissues. A: ventricle; B: Purkinje fiber; C: Atrium

Tissus	τ_0^{AP}	τ_{final}^{AP}	$J(\tau_{final}^{AP})$
A	[9, 0.1, 0.002, 0.02, 0.4]	[0.9633413, 0.0932280, 0.0078559, 0.019058, 1.5755477]	0.14932
B	[8, 0.1, 0.002, 0.03, 0.4]	[0.8677110, 0.0375976, 0.0080940, 0.1549662, 1.0769253]	0.28845
C	[6, 0.7, 0.009, 0.03, 0.3]	[2.0364918, 0.0744077, 0.0198289, 0.0364243, 0.4670758]	0.10828

Each line of the table 5 reads as follows, for example for the first line: starting from $\tau_0^{AP} = [9, 0.1, 0.002, 0.02, 0.4]$ to initialize the Nelder-Mead algorithm in the minimization of the function (5.2), we performed 627 iterations until convergence $\mid \tau_{k+1} - \tau_k \mid < 10^{-4}$, we got

$$\tau_{final}^{AP} = [0.9633413, 0.0932280, 0.0078559, 0.019058, 1.5755477]$$

and $J(\tau_{final}^{AP}) = 0.14932$.

As illustrated in figure 7, it can be seen that the potential u of the Aliev-Panfilov model fits quite well to the potential $\tilde{u}$ obtained from the Mitchell-Schaeffer model in the three heart tissues. This allows us to affirm that we have correctly identified the parameters of the Aliev-Panfilov model and that it can be used in these three regions of the heart to predict the trans-membrane potential. Again, the v gate variable fit is not as good. Indeed, phase 4 predicted by the Aliev-Panfilov and Mitchell-Schaeffer models lasts, respectively, $\Delta T_4 =$ 400 ms and $\Delta T_4 =$ 700 ms in the ventricle, $\Delta T_4 =$ 200 ms and $\Delta T_4 =$ 800 ms in the Purkinje fibers, $\Delta T_4 =$ 150 ms and $\Delta T_4 =$550 ms in the atria. The recovery phase predicted by Aliev-Panfilov with this parameter adjustment method is therefore 2 to 4 times too short. The duration of phase 4 predicted by Mitchell-Schaeffer had been adjusted to the experimental values in ([11, 12]), so this value is considered more reliable than for Aliev-Panfilov.

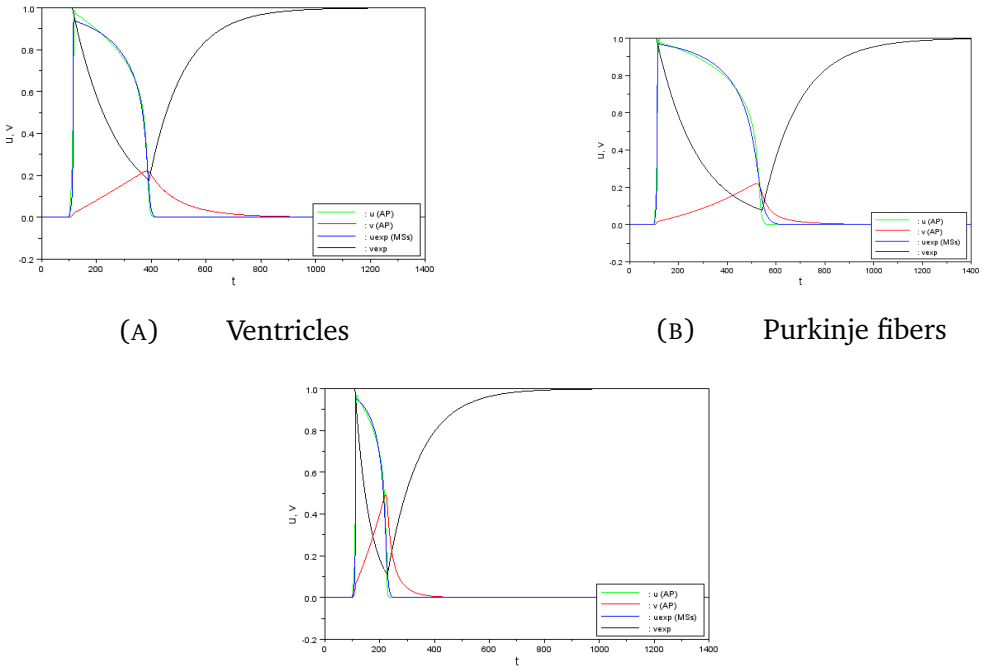

(A) Ventricles (B) Purkinje fibers

(C) Atrium

FIGURE 7. Solutions of the Aliev-Panfilov model fitted to those of the Mitchell-Schaeffer model in three cardiac tissues.

5.3. **Comparison of Fenton-Karma and Standard Mitchell-Schaeffer Ionic Models.** We want to adjust the potential u of the Fenton-Karma model to the potential $\tilde{u}$ obtained using the standard Mitchell-Schaeffer model. As the standard Mitchell-Schaeffer model derives from that of Fenton-Karma, we will also seek to verify the adjustment of w of the Fenton-Karma model on $\tilde{v}$ of Mitchell-Schaeffer since w and v of Fenton-Karma and Mitchell-Schaeffer, respectively, admit similar behavior. To adjust the Fenton-Karma potential u to the Mitchell-Schaeffer potential $\tilde{u}$, we minimized the function $J = J(\tau)$ given in (5.2) by setting $\tau_0^{FK} = [0.2, 120, 125, 8, 10, 9000, 80]$ to initialize the Nelder-Mead algorithm. Then we got

$$\tau_{final}^{FK} = [0.3371032, 106.40989, 132.45111, 2.67672, 9.6557978, 1034.8688, 46.82292]\,,$$

for which

$$J(\tau_{final}^{FK}) = 3.2422036.$$

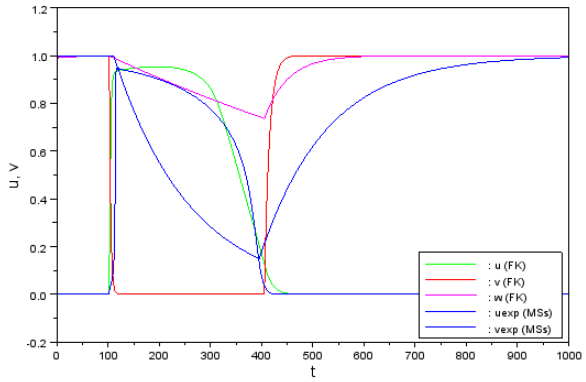

FIGURE 8. Graph illustrating the adjustment of the Fenton-Karma model on that of Mitchell-Schaeffer.

Figure 8 illustrates that fitting the Fenton-Karma and Mitchell-Schaeffer potentials u and $\tilde{u}$, respectively, is good for the overall aspect of the action potential. In particular, the durations of the phases of depolarization, repolarization and, to a lesser extent of the tray are very close for the two potentials u and $\tilde{u}$. However, the potential of the Fenton-Karma model is flatter at the start of phase 2 (the tray) and drops more rapidly at the start of phase 3 (the repolarization) compared to the Mitchell-Schaeffer model. we will notice, however, that the return to equilibrium of the recovery variables w and $\tilde{v}$ predicted by the Fenton-Karma and Mitchell-Schaeffer models, respectively, takes place almost at the same speed.

5.4. **Comparison of Standard Mitchell-Schaeffer and Beeler-Reteur Ionic Models.** In this section we want to fit the potential u of the standard Mitchell-Schaeffer model to the potential $\tilde{u}$ obtained using the Beeler-Reuter model [2]. The solution $\tilde{u}$ of the Beeler-Reuter model was generated according to the numerical methods described in [14]. The particularity of the Beeler-Reuter model compared to the other models defined in the 4 section is that, its potential presents a slight peak between the end of the first phase (the ”depolarization” phase) and the beginning of the second phase (tray phase). Immediately after depolarization, there is a rapid drop in potential, which then rises slightly before completing the tray phase. To adjust the Mitchell-Schaeffer potential u to the Beeler-Reuter potential $\tilde{u}$, we minimized the function $J = J(\tau)$ given in (5.2) by setting $\tau_0^{MS} = [0.27, 5.8, 128, 129]$ to

initialize the Nelder-Mead algorithm. Then we got,

$$\tau_{final}^{MS} = [0.0373243, 7.7090625, 249.64664, 57.812497]\,,$$

for which

$$J(\tau_{final}^{MS}) = 3.4381449.$$

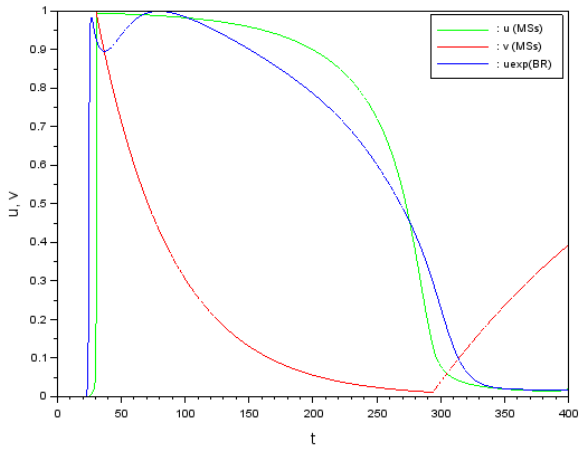

FIGURE 9. Graph illustrating the adjustment of the Mitchell-Schaeffer model on that of Beeler-Reteur.

Figure 9 illustrates that fitting the Mitchell-Schaeffer and Beeler-Reuter potentials u and $\tilde{u}$, respectively, is good for the overall aspect of the action potential. In particular, the durations of the depolarization, repolarization and tray phases are very close for the two potentials u and $\tilde{u}$. However, the potential $\tilde{u}$ of the Beeler-Reuter model has a more complex shape than that of the standard Mitchell-Schaeffer potential u during phase 2. It is not possible to capture these details in the variation of u with the standard Mitchell-Schaeffer model for which the shape of the action potential remains quite simple. we will also notice the faster descent of the Mitchell-Schaeffer potential u during the repolarization phase compared to Beeler-Reuter.

5.5. **Comparison of Modified Mitchell-Schaeffer and Beeler-Reteur Ionic Models.** In this section we want to fit the potential u of the modified Mitchell-Schaeffer model to the potential $\tilde{u}$ obtained using the Beeler-Reuter model. The solution $\tilde{u}$

of the Beeler-Reuter model was generated according to the numerical methods described in [14]. The particularty of this comparison regarding to the one made in the section 5.4 is due to the fact that the modified Mitchell-Schaeffer potential u also presents a slight peak between the end of the first phase (the phase of "depolarization") and the beginning of the second phase (the "tray" phase) like that of Beller-Reuter. Although the potentials for modified Mitchell-Schaeffer and Beeler-Reuter show differences in the shape of this peak at the beginning of phase 2, we will still seek to adjust these two potentials. To adjust the Mitchell-Schaeffer potential u to the Beeler-Reuter potential $\tilde{u}$, we minimized the function $J = J(\tau)$ given in (5.2) by setting $\tau_0^{MSm} = [0.25, 6.3, 2.2, 20, 218, 300, 0.033, 20000]$ to initialize the Nelder-Mead algorithm. Then we got,

$$\tau^{MSm} = [0.0822240, 2.0417859, 4.7774742, 18.648936, 222.70821, 638.26143, 0.0211528, 40584.463]$$

for which

$$J(\tau_{final}^{MSm}) = 0.2455316$$

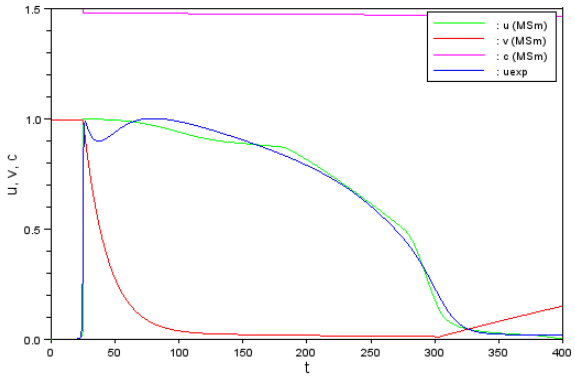

FIGURE 10. Graph illustrating the fit of the modified Mitchell-Schaeffer model to the Beeler-Reteur model.

Figure 10 illustrates that fitting the modified Mitchell-Schaeffer and Beeler-Reuter potentials u and $\tilde{u}$, respectively, is very good for the overall aspect of the action potential. In particular, the durations of the depolarization, repolarization and

tray phases are very close for the two potentials u and $\tilde{u}$. The modified Mitchell-Schaeffer potential u fits better the Beeler-Reuter potential $\tilde{u}$ compared to the standard Mitchell-Schaeffer potential, which is confirmed by $J(\tau_{final}^{MSm}) < J(\tau_{final}^{MS})$ by at least an order of magnitude.

6. COVER THE SHAPE OF THE WAVE OBTAINED EXPERIMENTALLY BY FLUORESCENCE EFFECT ON PIGS

We present action potentials measured at the Medical Biophysics Laboratory of the University of Toronto, Canada [10]. These measurements were carried out on pigs using the technique of optical imaging by fluorescence effect [4, 5]. The figure 11 illustrates the measured and normalized potentials (between 0 and 1) over time t (in ms). Figure 11a shows several action potentials for a heart beating at 70 beats per minute. We targeted one of the action potentials of the figure 11a to define the potential $\tilde{u}$ used to adjust the parameters (see figure 11b). Then we isolated this portion of the graph, which constitutes our experimental potential $\tilde{u}$ in order to adjust the potentials u of the Mitchell-Schaeffer and Aliev-Panfilov models using $Scilab$.

We fit the u potentials of the standard Mitchell-Schaeffer and Aliev-Panfilov models to the $\tilde{u}$ potential obtained using the experimental data in figure 11c using the function $J = J(\tau)$ given in (5.2). Starting from the conditions $\tau_0^{MS} = [0.38, 8, 135, 160]$ and $\tau_0^{AP} = [8.5, 0.15, 0.001, 0.02, 0.4]$ to initialize the Nelder-Mead algorithm for the standard Mitchell-Schaeffer and Aliev-Panfilov ionic models, respectively, we obtained

$$\begin{aligned} \tau_{final}^{MS} &= [2.0295711, 37.794847, 607.74009, 120.62614]\,, \\ J(\tau_{final}^{MS}) &= 0.2773095, \\ \tau_{final}^{AP} &= [8.5085251, 0.0938535, 0.0010674, 0.0205510, 0.4799080]\,, \\ J(\tau_{final}^{AP}) &= 8.8515504. \end{aligned}$$

As illustrated in figure 12, it can be seen that the potential u of the standard Mitchell-Schaeffer model fits better on the potential $\tilde{u}$ obtained by fluorescence than that of Aliev- Panfilov. This is confirmed by the fact that $J(\tau_{final}^{AP}) > J(\tau_{final}^{MS})$, that is to say, the adjustment error $\| u - \tilde{u} \|_{L^2(0,T)}$ is larger for the Aliev-Panfilov

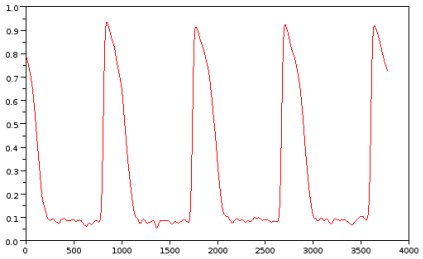

(A) Experimentals data

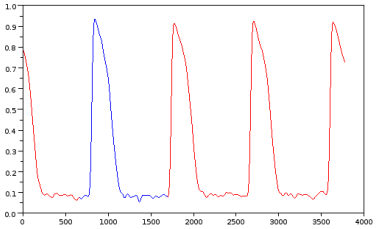

(B) Extraction of the wave

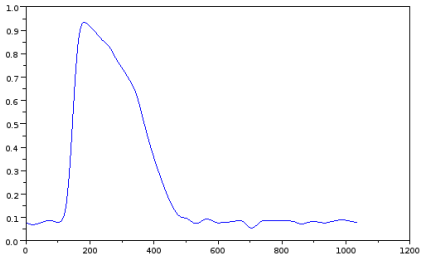

(C) The isolated wave

FIGURE 11. Trans-membrane potential $\tilde{u}$ (normalized) measured by fluorescence as a function of time t (in ms).

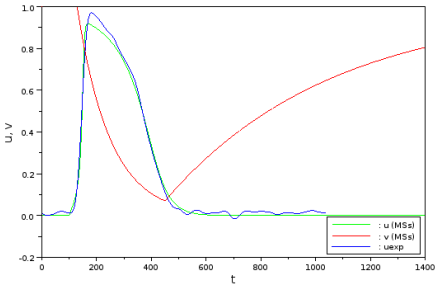

(A) Adjusted u from MS to $\tilde{u}$ from pigs

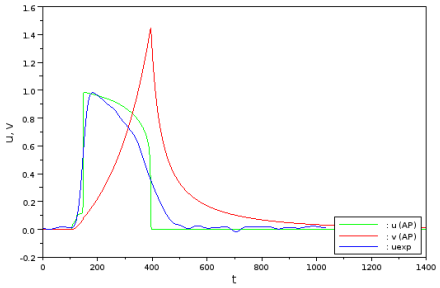

(B) Adjusted u of AP on $\tilde{u}$ of pigs

FIGURE 12. Adjustments of the Mitchell-Schaeffer and Aliev-Panfilov potentials u on an experimentally measured potential $\tilde{u}$.

model than the standard Mithcell-Schaeffer. Once again the gate variables v do not behave the same way for the two models. The Aliev-Panfilov model predicts a phase 4 (from the end of depolarization to the return of v to equilibrium) between

$T_4 = 550\ ms$ and $T_5 = 1200\ ms$, that is to say, a duration $\Delta T_4 = 650\ ms$. On the other hand, phase 4 predicted by standard Mitchell-Schaeffer model is superior to $700ms$. The experimental value of the phase 4 duration is not known.

7. Conclusion and perspectives

In this article, we have defined an optimization problem allowing to directly find the shape of the cardiac wave of some ionic models. This allowed us to compare some of these ionic models via a parameter identification problem instead of comparing them directly by plotting the graphs for given values of the parameters. Compared to the empirical methods used to adjust one or two parameters at a time encountered in electrophysiology, we also believe that we are the first to define a reliable identification problem able to simultaneously identify four to eleven parameters of an ionic model. Finally, we adjusted the parameters of the Mitchell-Scaheffer and Aliev-Panfilov models to find the shape of the action potential obtained experimentally by fluorescence. The Aliev-Panfilov model was manually fitted to these experimental data. Our approach has shown that the Mitchell-Schaeffer model fits the data better than the Aliev-Panfilov model. In order to better understand the duration of the recovery phase, it would be interesting to add a term of the least squares type depending on the numerical and experimental phase 4 durations (in the cost function making it possible to adjust the shape of the wave) in order to adjust the gate variables v of ionic models. Finally, we have in view to define another identification problem in order to adjust the restitution curves of certain ionic models. We also foresee the future application of this kind of parameter identification methods to all sorts of problems (for example, in fluid mechanics for the oil industry).

Acknowledgment

The authors thank the anonym referees of Advances in Mathematics: Scientific Journal, for their valuable comments and suggestions which have led to an improvement of the presentation.

REFERENCES

[1] R.R. ALIEV, A.V. PANFILOV: *Reconstruction of the action potential of ventricular myocardial fibres*, J. of Physi., **268**(1) (1977), 177-210.

[2] G.W. BEELER, H. REUTER: *Reconstruction of the action potential of ventricular myocardial fibres*, J. of Physi., **268**(1) (1977), 177-210.

[3] F. FENTON, A. KARMA: *Vortex dynamics in three-dimensional continuous myocarduim with fiber rotation: Filament instability and fibrillation.*, Chaos, **8** (1998), 20-47.

[4] I.R. EFIMOV, V.P. NIKOLSKI, G. SALAMA: *Optical imaging of the heart*, Circulation research **95** (2004), 21-33.

[5] I.R. EFIMOV, T.D. HUANG, J.M. RENDT, G. SALAMA : *Optical mapping of repolarization and refractoriness from intact heart*, Circulation research **90** (1994), 1469-1480.

[6] J.D. FAIRES, R. BURDEN: *Numerical methods*, 2nd ed., Pacific Grove, CA, 1998.

[7] K. JAIN, P. MIAHELA, H. DELINGETTE, G. WRIGHT, N.M. SERMESANT: *Personalization of a cardiac electrophysiologic model using optical mapping and MIR for prediction of changes with pacing*, IEEE, Trans. Biomed. Eng. **10**(10) (2011), 1-11.

[8] K. JAIN, ET AL: *Coupled personalization of cardiac electrophysiology models for prediction of ischaemic ventricular tachycardia.*, Interface Focus **1** (2011), 396–407.

[9] C.C. MITCHELL, D.G. SCHAEFFER.: *A two-current model for the dynamics of cardiac membrane*, Bulletin of Mathematical Biology, **65**(5) (2003), 767-793.

[10] P, MIAHELA, ET AL.: *Fusion of optical imaging and MRI for the evaluation and adjustment of macroscopic models of cardiac electrophysiology: a feasibility study.*, Med. Image Anal. **13**(2) (2009), 370-80.

[11] D.V. PONGUI NGOMA, Y. BOURGAULT, H. NKOUNKOU: *Parameter identification for a non-differentiable ionic model used in cardiac electrophysiology.*, Appl. Math. Sci. **150**(9) (2015), 7483-7507.

[12] D.V. PONGUI NGOMA, Y. BOURGAULT, P. MIAHELA, H. NKOUNKOU: *Adjustment of Parameters in ionic models using optimal control problems*, FIMH, **10263** (2017), 322-332.

[13] M. RIOUX, Y. BOURGAULT: *A predictive method allowing the use of a single ionic model in numerical cardiac electrophysiology*, Math. Model. and Numer. Anal. **47** (2013), 987-1016.

[14] T. ROY, Y. BOURGAULT, C. PIERRE: *Analysis of time-stepping methods for the monodomain model*, Hal Open Science, (2020), 1-35.

[15] D.G. SCHAEFFER, ET AL: *An inonically based mapping model with memory for Cardiac restitution*, Bull. of math. biol., **69** (2007), 459-482.

[16] D.G. SCHAEFFER, ET AL: *Asymptotic approximation of an ionic model for cardiac restitution*, Kl. Acad. Publ. **20**(23) (2006), 1-16.

[17] E.G. TOLKACHEVA,ET AL: *Analysis of the Fenton- Karma model through an approximation by a one-dimensional map*,Chaos. **4**(12) (2002), 1034-1042.

ECOLE NATIONALE SUPERIEURE POLYTECHNIQUE
MARIEN NGOUABI UNIVERSITY
AVENUE DE PREMIER JEUX AFRICAINS, BRAZZAVILLE,
CONGO.
Email address: diogene.ponguingoma@umng.cg

ECOLE NORMALE SUPERIEURE
MARIEN NGOUABI UNIVERSITY
AVENUE DE PREMIER JEUX AFRICAINS, BRAZZAVILLE,
CONGO.
Email address: vital.mabonzo@umng.cg

ECOLE NATIONALE SUPERIEURE POLYTECHNIQUE
MARIEN NGOUABI UNIVERSITY
AVENUE DE PREMIER JEUX AFRICAINS, BRAZZAVILLE,
CONGO.
Email address: landry.gomat@umng.cg

ECOLE NATIONALE SUPERIEURE POLYTECHNIQUE
MARIEN NGOUABI UNIVERSITY
AVENUE DE PREMIER JEUX AFRICAINS, BRAZZAVILLE,
CONGO.
Email address: germain.nguimbi@umng.cg

ECOLE NATIONALE SUPERIEURE POLYTECHNIQUE
MARIEN NGOUABI UNIVERSITY
AVENUE DE PREMIER JEUX AFRICAINS, BRAZZAVILLE,
CONGO.
Email address: bervi84@gmail.com